Applied Mathematical Modelling 37 (2013) 5215–5226

Contents lists available at SciVerse ScienceDirect

Applied Mathematical Modelling

journal homepage: www.elsevier.com/locate/apm

Integration of barotropic vorticity equation over spherical geodesic grid using multilevel adaptive wavelet collocation method

Ratikanta Behera, Mani Mehra *

Department of Mathematics, Indian Institute of Technology Delhi, New Delhi 110016, India

ARTICLE INFO

Article history:
Received 16 February 2012
Received in revised form 17 September 2012
Accepted 15 October 2012
Available online 27 October 2012

Keywords:
Wavelets
Barotropic equation
Multilevel methods

ABSTRACT

In this paper, we present the multilevel adaptive wavelet collocation method for solving non-divergent barotropic vorticity equation over spherical geodesic grid. This method is based on multi-dimensional second generation wavelet over a spherical geodesic grid. The method is more useful in capturing, identifying, and analyzing local structure [1] than any other traditional methods (i.e. finite difference, spectral method), because those methods are either full or partial miss important phenomena such as trends, breakdown points, discontinuities in higher derivatives of the solution. Wavelet decomposition is used for interpolation and adaptive grid refinement on different levels.

© 2012 Elsevier Inc. All rights reserved.

1. Introduction

The barotropic vorticity equation model is an important equation in the research of the atmospheric sciences which describes the evolution of the vorticity of a fluid element as it moves around. It is a simplification of conservation law of momentum for inviscid and incompressible fluid. For the theoretical investigations of the evolution of vortices, atmospheric researchers are using the barotropic assumption, as there is no vertical component, i.e., single-layered fluid. Moreover, barotropic model is useful for modeling the movement of tropical cyclones [2–4] and the interaction of two vortices in close proximity to one another [5]. The barotropic assumption has also been used to model global wave patterns in the middle troposphere [6,7]. But sometime to find analytic solutions of these type of problems are either not known or very difficult to develop. Therefore, many scientists pay attention to the research of numerical methods of the equation [8–10].

Since atmospheric blockings are approximately stationary and relatively long-lived phenomena, so that one might attempt to describe them in term of stationary solution of barotropic vorticity equation [11,12]. However the baropropic vorticity equation on a sphere has known several stationary or longitudinally propagating solution, such as exact solution of Rossby–Hauritz wave [13] and modons [14,15]. Examples of numerical solution obtained for Rossby–Hauritz wave [16] and modons [17,14]. This solution of modon and Rossby–Hauritz is to be presented here with less computational cost and clearly indicating the region of sharp gradient.

The theory and application of wavelets has become an active area of research in different fields, including electrical engineering (signal processing, data compression), mathematical analysis (harmonic analysis, operator theory), and physics (fractals, quantum field theory). Moreover, it also applied to seismic signal studies in geophysics; and applications in turbulence studies in the atmospheric sciences. Basically application of signal analysis in atmosphere sciences has two main directions as followed: the singularity and the variance analysis.

* Corresponding author.
E-mail addresses: ratikanta_ma@student.iitd.ac.in (R. Behera), mmehra@maths.iitd.ac.in (M. Mehra).

0307-904X/$ - see front matter © 2012 Elsevier Inc. All rights reserved.
http://dx.doi.org/10.1016/j.apm.2012.10.027

The current wavelet method can be classified in different ways depending on the above applications whether it take full or partial advantage of wavelet analysis (i.e. multiresolution properties, wavelet compression, the detection of localized structures and subsequent use for grid adaptation, fast wavelet transform, wavelet-based interpolation, and active error control) [18]. But still now it's application for solving partial differential equations (PDEs) on general manifold is in infancy stage. A new adaptive second generation wavelet collocation method for solving PDEs on sphere has recently been developed in [19]. The adaptive wavelet collocation method is most appropriate for solving nonlinear PDEs with general boundary conditions. This approach combines the adaptivity and error control of the adaptive wavelet method with the flexibility of collocation. It has been verified by many authors in [20,21,1,22,23] over the flat geometry and [19,24] on sphere. Therefore, the aim of this paper is to apply multilevel adaptive wavelet collocation method (MAWCM) for solving useful barotropic vorticity equation on the sphere. Since wavelets are localized in both space and scale, we can clearly analyze local structure of any kind. Furthermore the computational cost of the MAWCM is $O(\mathcal{N})$ which is independent of the dimension of the problem, where $\mathcal{N}$ is the total number of collocation points.

The paper is organized as follows, the brief introduction about second generation wavelet is given in Section 2. In Section 3, we are discussing MAWCM to solve PDEs on the sphere. Moreover in section 4 we describe clearly how operators (Jacobian operator and Laplace–Beltrami operator) are calculated on an adaptive grid. In Section 5, the numerical experiment of two test cases are given. The conclusion is outlined in Section 6.

2. Spherical wavelets

Some of the first non-trivial wavelets that have been developed are the Daubechies wavelet [25], Coiflets [25,26], Meyer wavelet [27] and Morlet wavelet [25,28]. These, and most other wavelets developed in the 1980s, are first generation wavelets whose construction requires the Fourier transform and whose basis functions have to be dilation and translation of single function (mother wavelet). However, these wavelets were limited to flat geometries. The work by Swelden [29] overcome these restrictions and led to the second generation wavelets on general manifold.

The construction of spherical wavelet (second generation wavelet) in [30] relies on recursive partitioning of the sphere into spherical triangles. This is done staring from a platonic solid whose faces are spherical triangles. Here we consider the icosahedral subdivision for which $\mathcal{K}^j = 10 \times 4^j + 2$ at subdivision level j. Let $\mathcal{S}$ be a triangulation of the sphere S and denote the set of all vertices obtained after subdivisions with $\mathcal{S}^j = \{p_k^j \in S | k \in \mathcal{K}^j\}$, where $\mathcal{K}^j$ is an index set. Now the original platonic solid icosahedral $\mathcal{S}^0$ contains only 12 vertices and the $\mathcal{S}^1$ contains those vertices and all new vertices on the edge midpoints. Since $\mathcal{S}^j \subset \mathcal{S}^{j+1}$ we also let $\mathcal{K}^j \subset \mathcal{K}^{j+1}$. Let $\mathcal{M}^j = \mathcal{K}^{j+1}/\mathcal{K}^j$ be the indices of the vertices added when going from level j to $j+1$.

A second generation multi resolution analysis (MRA) [29] of the sphere provides a sequence $\mathcal{V}^j \subset L_2(S)$ with $j \geqslant 0$; and the sphere $S = \{p = (p_x, p_y, p_z) \in \mathbb{R}^3 : \|p\| = r\}$, where r is the radius of the sphere:

- $\mathcal{V}^j \subset \mathcal{V}^{j+1}$,
- $\bigcup_{j \geqslant 0} \mathcal{V}^j$ is dense in $L_2(S)$,
- each $\mathcal{V}^j$ has a Riesz basis of scaling functions $\{\phi_k^j | k \in \mathcal{K}^j\}$.

Since $\phi_k^j \in \mathcal{V}^j \subset \mathcal{V}^{j+1}$, for every scaling function ϕ_k^j filter coefficients $h_{k,l}^j$ exists such that

$$\phi_k^j = \sum_{l \in \mathcal{K}^{j+1}} h_{k,l}^j \phi_l^{j+1}. \tag{1}$$

Note that the filter coefficients $h_{k,l}^j$ can be different for every $k \in \mathcal{K}^j$ at a given level $j \geqslant 0$. Therefore each scaling function satisfies a different refinement relation. Each MRA is accompanied by a dual MRA consisting of nested spaces $\tilde{\mathcal{V}}^j$ with bases by the dual scaling functions $\tilde{\phi}_k^j$, which are biorthogonal to the scaling functions:

$$\langle \phi_k^j, \tilde{\phi}_{\acute{k}}^j \rangle = \delta_{k,\acute{k}}, \quad \text{for } k, \acute{k} \in \mathcal{K}^j, \tag{2}$$

where $\langle f, g \rangle = \iint_S fg dw$ is the inner product on the sphere. The dual scaling functions satisfy refinement relations with coefficients $\{\tilde{h}_{k,l}^j\}$. The surface plot of scaling function and it's cross cut along maximum and minimum are plotted in Fig. 1.

One most important thing when you are going to build MRA to construction of wavelets. They encode the difference between two successive levels of representation, that is there from Riesz basis for the space $\mathcal{W}$, which is complement of $\mathcal{V}^j$ in $\mathcal{V}^{j+1}$ (i.e. $\mathcal{V}^{j+1} = \mathcal{V}^j \oplus \mathcal{W}^j$). The construction of the wavelets form a Riesz basis for $L^2(S)$ and allow a function to be represented by its wavelet coefficients. Since $\mathcal{W}^j \subset \mathcal{V}^{j+1}$, we can write

$$\psi_k^j = \sum_{l \in \mathcal{K}^{j+1}} g_{k,l}^j \phi_l^{j+1}, \tag{3}$$

and the spherical wavelets ψ_m^j have $\tilde{d}$ vanishing moments, if $\tilde{d}$ is the independent polynomials P_i, $0 \leqslant i \leqslant \tilde{d}$ exist such that

$$\langle \psi_m^j, P_i \rangle = 0 \quad \forall j \geqslant 0,\ m \in \mathcal{M}^j, \tag{4}$$

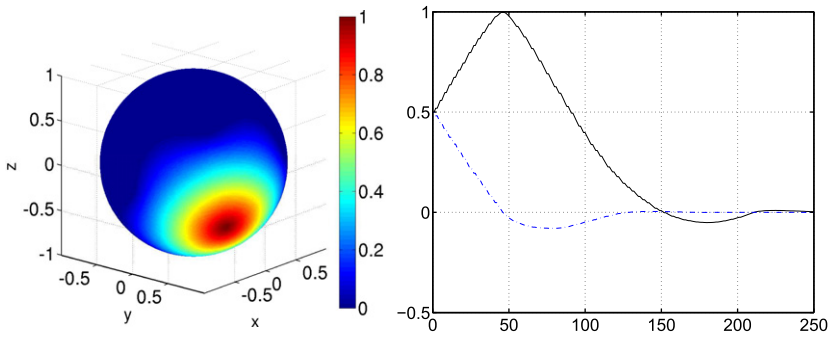

(a) Scaling function (b) Cross cut of scaling function along the maximum and minimum

Fig. 1. (a) Scaling function; (b) cross cut of scaling function along the maximum and minimum.

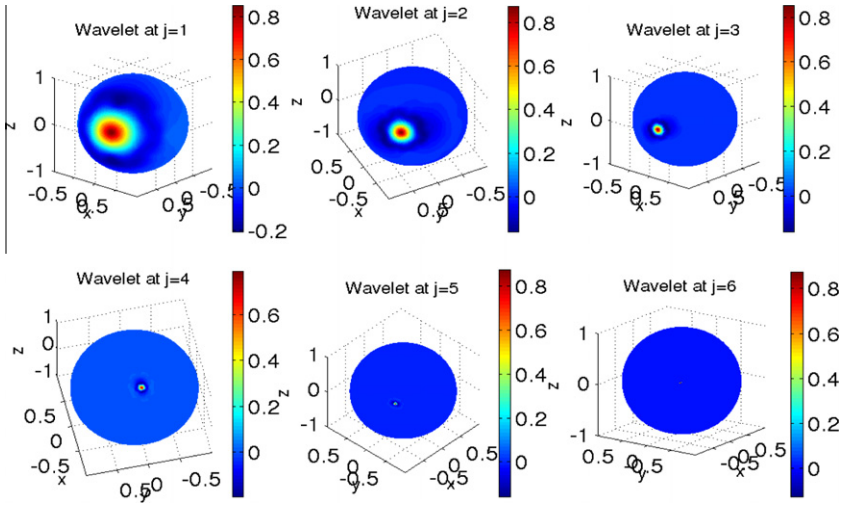

Fig. 2. Wavelets at different levels (j).

where $\mathcal{M}^j$ is the index set and polynomial P_i are define as the restriction to the sphere of polynomials on $\mathbb{R}^3$. We also plot wavelets at different scales in Fig. 2 and cross cut of wavelets along the maximum in Fig. 3. One thing to observe from Fig. 3 that wavelets are more localized with increasing j.

3. Multilevel adaptive wavelet collocation method

The main advantage of wavelet decomposition is it's ability to compress the function. For functions which contain isolated small scales on a large scale background, most wavelet coefficients will be small and by discarding a large number of these small coefficients, we can efficiently approximate the function.

Consider a function $u(p) \in L_2(S)$ which can be approximated as

$$u(p) = \sum_{k\in\mathcal{K}^0} c_k^0 \phi_k^0(p) + \sum_{j=0}^{\infty} \sum_{m\in\mathcal{M}^j} d_m^j \psi_m^j(p). \tag{5}$$

This equation can be written as sum of two terms composed of wavelets whose amplitudes are, above and below some prescribed threshold ϵ that is

$$u(p) = u_{\geqslant}(p) + u_{<}(p), \tag{6}$$

$$\text{where } u_{\geqslant}(p) = \sum_{k\in\mathcal{K}^0} c_k^{J_0} \phi_k^{J_0}(p) + \sum_{j=J_0}^{\infty} \sum_{\substack{m\in\mathcal{M}^j \\ |d_m^j|\geqslant\epsilon}} d_m^j \psi_m^j(p), \tag{7}$$

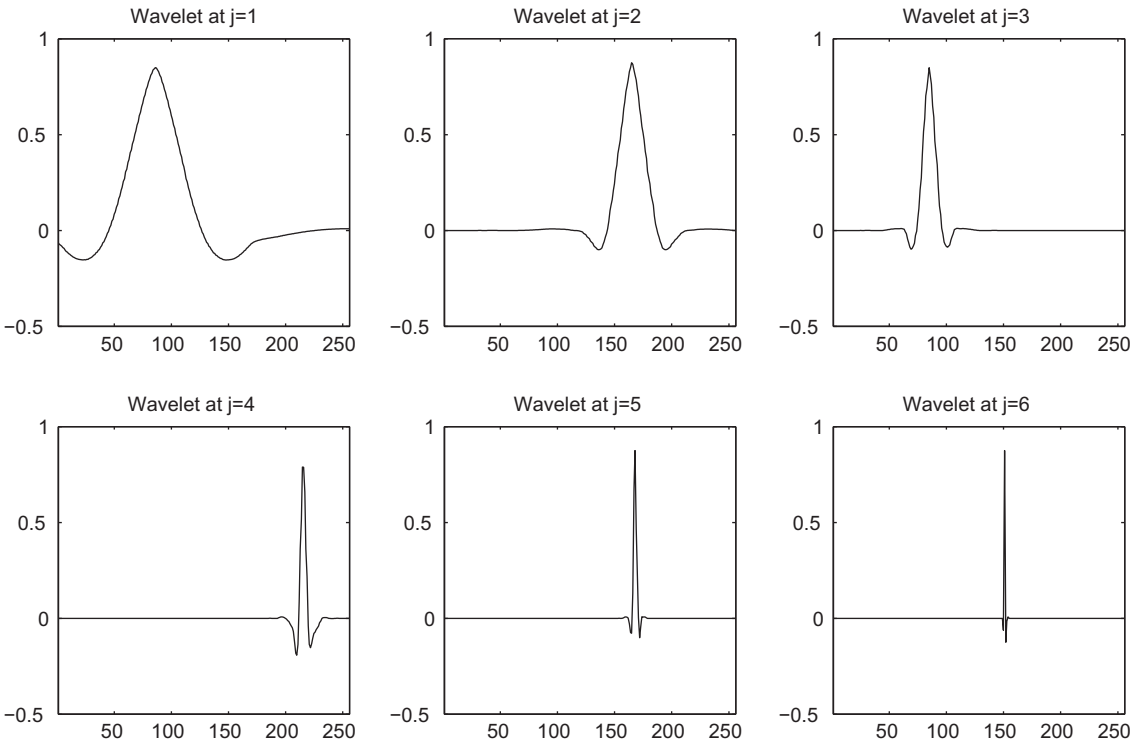

Fig. 3. Cross section of Fig. 2 along the maximum.

$$u_{<}(p) = \sum_{j=J_0}^{\infty} \sum_{\substack{m \in \mathcal{M}^j \\ |d_m^j| < \epsilon}} d_m^j \psi_m^j(p), \tag{8}$$

where J_0 is the coarse level of approximation, Donoho [31] has shown that for smooth enough u,

$$\|u(p) - u_{\geqslant}(p)\|_{\infty} \leqslant c_1 \epsilon, \tag{9}$$

and the number of significant coefficients $N(\epsilon) = \mathcal{N}$ depends on ϵ,

$$N(\epsilon) \leqslant c_2 \epsilon^{-n/d}, \tag{10}$$

where d is the order of interpolation, n is the dimension of the problem and the coefficients c_i's depend on the function. Combining relations (9) and (10) gives the following bound on the error in terms of $N(\epsilon)$

$$\|u(p) - u_{\geqslant}(p)\|_{\infty} \leqslant c_3 N(\epsilon)^{-d/n}. \tag{11}$$

Note that d controls the number of zero moments of the interpolating scaling function. This error estimate is consistent with numerical experiment for flat geometry (Vasilyev and Bowman [21,1]), and (Mehra and Kevlahan in [19]) on the sphere.

In order to realize the benefits of the wavelet compression, we need to have the ability to reconstruct $u_{\geqslant}(p)$ from the subset of $N(\epsilon) \subset N$ of significants grid points. Furthermore, we recall that every wavelet $\psi_i^j(x)$ is uniquely associated with a collocation point. Hence once the wavelet decomposition is performed, each grid point is uniquely associated either with the wavelet or scaling function at the coarsest level of resolution. Consequently, the collocation point should be omitted from the computational grid, if the associated wavelet is omitted from the approximation. This procedure results in a set of nested adaptive computational grids $\mathcal{S}_{\geqslant}^j \subset \mathcal{S}^j$, such that $\mathcal{S}_{\geqslant}^j \subset \mathcal{S}_{\geqslant}^{j+1}$, for any $j < J - 1$, where J is the finest level of resolution present in approximation $u_{\geqslant}(x)$ (for detail see in one dimensional and multi dimensional [21,1] and on the sphere [19]). Thus, if there are no points in the immediate vicinity of a grid point p_i^j, means $|d_k^j| \leqslant \epsilon$ for all $k \in N(i)$, and the points $p_k^{j+1}, k \in N(i)$, are not present in $\mathcal{S}^{j+1}$, then there exists some neighborhood Ω_i^j of p_i^j, where the function can be interpolated by a wavelet interpolant based on $s_{k,m}^j (k \in \mathcal{K}_m)$:

$$\left| u(p) - \sum_{k \in \mathcal{K}(i)} s_{k,m}^j \phi_k^j(p) \right| \leqslant c_3 \epsilon, \tag{12}$$

where the coefficients $s_{k,m}^j$ can be chosen according as [19].

When solving the evolution equations an additional criterion for grid adaptation should be added. The computational grid should consist of grid points associated with wavelets whose coefficients are significant or could become significant during a time step. In other words, at any instant in time, the computational grid should include points associated with wavelets belonging to an adjacent zone of wavelets for which the magnitude of their coefficients is greater than an a priori prescribed threshold.

4. Operators on an adaptive grid

The barotropic vorticity equation describing the time evolution of two-dimensional non-divergent incompressible and inviscous flow, for a rotating spherical geometry can be written as

$$\begin{aligned} &\frac{\partial \zeta}{\partial t} = -J_s(\psi, \zeta + f), \\ &\zeta = \Delta\psi. \end{aligned} \tag{13}$$

Here $\zeta(\theta, \phi, t)$ is the vorticity (relative vorticity) of the horizontal wind on the surface of the sphere. where $-\pi \leqslant \theta \leqslant \pi$ and $-\pi/2 \leqslant \phi \leqslant \pi/2$ are longitude and latitude, respectively, ψ is the stream function, f is the Coriolis parameter, t is the time and Δ is the Laplace–Beltrami operator on the sphere, which is defined as

$$\Delta\alpha = \frac{1}{r^2 \cos^2\phi}\left[\frac{\partial^2 \alpha}{\partial\theta^2} + \cos\phi \frac{\partial}{\partial\phi}(\cos\phi \frac{\partial\alpha}{\partial\phi})\right], \tag{14}$$

and the Jacobian operator J_s on a sphere is defined as

$$J_s(\alpha, \beta) = \frac{1}{r^2 cos\phi}\left[\frac{\partial\alpha}{\partial\theta}\frac{\partial\beta}{\partial\phi} - \frac{\partial\beta}{\partial\theta}\frac{\partial\alpha}{\partial\phi}\right], \tag{15}$$

where α, β are any two scalar function, r is the radius of the sphere. When we are solving barotropic vorticity equation, it is necessary to approximate differential operators (i.e. Laplace–Beltrami (Eq. (14)) and Jacobian (Eq. (15))) at collocation points. For spherical Poisson equation, the convergence of Laplace–Beltrami operator on an spherical geodesic grid [32] is presented in [24]. First, we will study the convergence of Jacobian operator on an spherical geodesic grid and secondly MAWCM will be applied on barotropic vorticity equation. In this section we describe an efficient procedure for approximating Jacobian operator and Laplace–Beltrami operator [19].

Let p_i^j be a vertex of the triangulation at resolution j; and $p_k^j, \in N(i)$ be the neighboring vertices around p_i^j . The numerical approximation of the Laplace–Beltrami operator on the sphere S as proposed in [33] is then vortices

$$\Delta u = \frac{1}{A_s(p_i^j)} \sum_{k\in N(i)} \frac{\cot\alpha_{i,k} + \cot\beta_{i,k}}{2}\left[u(p_k^j) - u(p_i^j)\right],$$

where the $\alpha_{i,k}$ and $\beta_{i,k}$ are the angles shown in Fig. 4, $N(i)$ is the set of nearest neighbor vertices of the vertex p_i^j. $A_s(p_i^j)$ is the area of the one-ring neighborhood given by

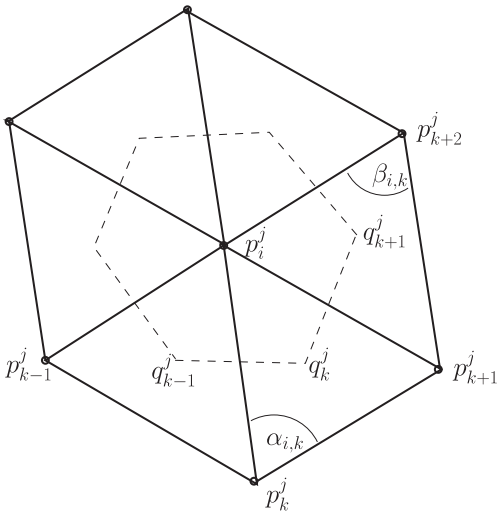

Fig. 4. Schematic figure of angles $\alpha_{i,k}, \beta_{i,k}$, neighboring vertices and area A_S used in evaluating derivatives on a spherical triangulation of a surface.

$$A_s(p_i^j) = \frac{1}{8}\sum_{k\in N(i)} (\cot\alpha_{i,k} + \cot\beta_{i,k})\|p_k^j - p_i^j\|^2.$$

Furthermore, the numerical approximation of the Jacobian operator over spherical geodesic grid [34] will be

$$J_s(u(p_i^j), v(p_i^j)) = \frac{1}{6A_s(p_i^j)}\sum_{k\in N(i)} (u(p_i^j) + u(p_k^j))(v(p_{k+1}^j) - v(p_{k-1}^j)), \tag{16}$$

The differentiation procedure is based on the interpolating properties of second-generation wavelets. Thus this procedure gives us the value of the Jacobian operator of the function at that particular location. The accuracy of the any function and its differentiation procedure was examined in [21,1] for flat geometries. Furthermore, Mehra and Kevlahan [19,24] have examined how to approximate a function on the sphere, and Laplace–Beltrami on the sphere. Here, the accuracy of the wavelet approximation of Jacobian operator is also being examined. Assume that we perform local differentiation at a point $p_k^j \in \mathcal{S}$ and h^j is the quality describing the local grid spacing in all directions at that point which is constant for a uniform grid, then from construction, the local truncation error of the interpolation scheme is $\|J_s u(p) - J_s u_{\geqslant}(p)\| = h^{(d-2)}$(loss of second order due to derivative), but $\|u(p) - u_{\geqslant}(p)\| = h^d = \epsilon$ (when one can filter any function) hence $h = \epsilon^{(1/d)}$ and

$$\|J_s u(p) - J_s u_{\geqslant}(p)\| \leqslant c_1\epsilon^{(1-2/d)} \leqslant c_2 N^{-(d-2)/2}, \tag{17}$$

for butterfly interpolation consistent with this relation $d = 4$

$$\|J_s u(p) - J_s u_{\geqslant}(p)\| \leqslant c_1\epsilon^{(1/2)} \leqslant c_2 N(\epsilon)^{-1}. \tag{18}$$

Now we have all the ingredients necessary to construct a dynamically adaptive during each time step for the solution of barotropic vorticity equation on the sphere. The three basic steps are as follows:

1. Knowing the solution $u_{\geqslant}(t)$ on the adaptive grid, we compute the values of wavelet coefficients corresponding to each component of the solution using the fast wavelet transform. For a given threshold ϵ. we update $\mathcal{S}_{\geqslant}^{t+\Delta t}$ based on the magnitude of wavelet coefficients. We also add an adjacent zone [19] to the significant coefficients to allow for the change in the solution during one time step, as described in Section 3.
2. If there is no change between computational grids $\mathcal{S}_{\geqslant}^{t}$ and $\mathcal{S}_{\geqslant}^{t+\Delta t}$, we go directly to next step. Otherwise we interpolate the values of the solution at the collocation points $\mathcal{S}_{\geqslant}^{t+\Delta t}$, which are not included in $\mathcal{S}_{\geqslant}^{t}$.
3. We integrate the resulting system of ordinary differential equations in time (e.g. using Runge–Kutta) to obtain new values to $u_{\geqslant}(t+\Delta t)$ at positions on adaptive grid $\mathcal{S}_{\geqslant}^{t+\Delta t}$, and go back to step 1.

5. Numerical results

5.1. Jacobian

Hear we are presenting how to calculate Jacobian in MAWCM by using initial solution [35] of both ζ and ψ.

$$\psi = -r^2\omega\sin\phi + r^2 K\cos^R\phi\sin\phi\cos R\theta, \tag{19}$$

$$\zeta = 2\omega\sin\phi - K\sin\phi\cos^R\phi(R^2+3R+2)\cos R\theta, \tag{20}$$

where $\omega = K = 7.8480\times10^{-6}s^{-1}$ and $R = 4$ are constant. Now we take $\epsilon = 10^{-5}$, and $r = 1$ and compute Jacobian $(J_s(\psi(p_i^j), \zeta(p_i^j)))$ using formula (16). The relation between $\|J_s u(p) - J_s u_{\geqslant}(p)\|_\infty$and ϵ is plotted in Fig. 5, here one can observe that error is of order $O(\epsilon)^{1/2}$ (verified against the theoretical predication (17), $d = 4$). Conclusively, the error is controlled by ϵ. The Jacobian of function ψ and ζ (as mentioned in Eqs. (19) and (20)) is plotted in the left of Fig. 6 and its adaptive grid is in right of Fig. 6. The adaptive grid in the right of Fig. 6 clearly indicating the region of sharp gradient.

To show the efficiency of MAWCM we need to compare number of grid points used in the adaptive and non adaptive grids. This can be measured by calculating compression coefficient $\mathcal{C} = N(\epsilon = 0)/N(\epsilon)$. In Fig. 6, the computed compression coefficient $\mathcal{C} = 3.14$ means we are computing Jacobian on adaptive grid which is having three times less number of grid points as compare to non adaptive (uniform) grid. Moreover from Fig. 7, one can observe that compression coefficient $\mathcal{C}$ increases when wavelet prescribed threshold parameter (ϵ) increases, means when ϵ goes to zero, the compression coefficient goes to one, i.e., adaptive algorithm becomes nonadaptive and its show the uniform (regular) grid. Therefore, adaptive grid clearly reflects the behavior of the function.

5.2. Test case-1

This test case is generally refer to Rossby–Haurwitz test case of shallow water test case [35]. For an initial vorticity equation (20), we plotted relation between ϵ and error and compared to the theoretical prediction [19] (i.e. $O(\epsilon)$, see in Fig. 8). Furthermore, the initial vorticity ζ and its adaptive grid are plotted in Fig. 9. Moreover, compression coefficient $\mathcal{C} = 77$. Again in Fig. 10, it is cleared that compression coefficient $\mathcal{C}$ increases when wavelet prescribed threshold parameter (ϵ) increases,

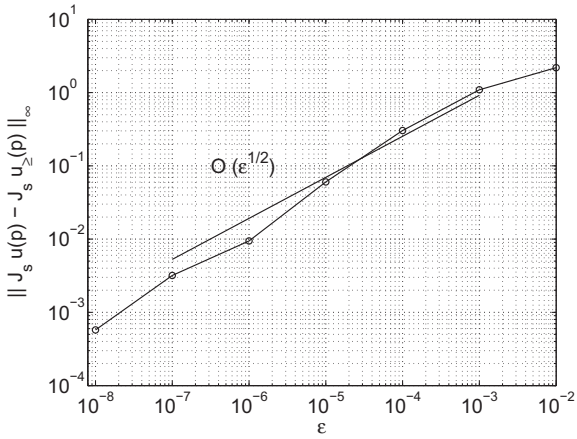

Fig. 5. Relation between ϵ and error $(\|J_s u(p) - J_s u_{\geqslant}(p)\|)$.

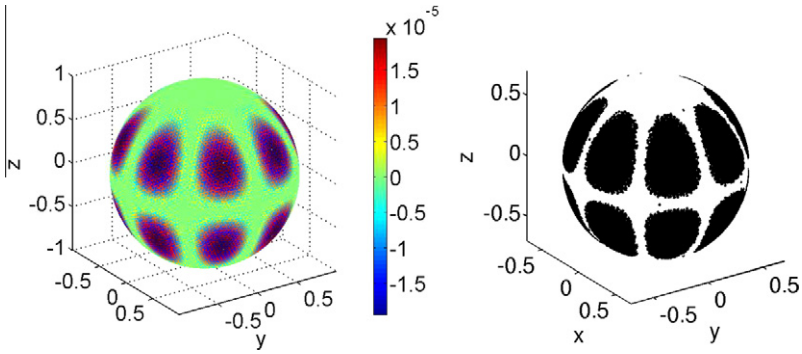

Fig. 6. Jacobian (left) and its adaptive grid (right).

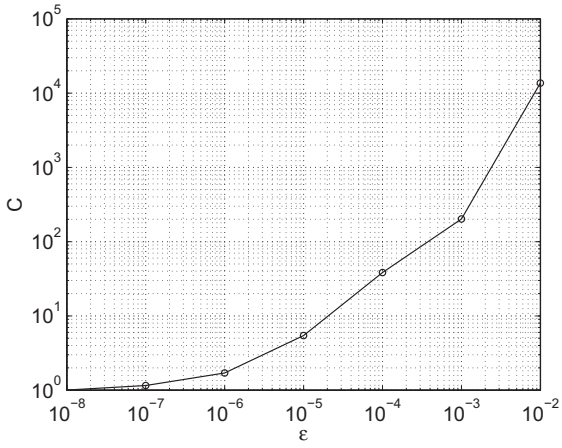

Fig. 7. Relation between compression coefficient $\mathcal{C}$ and ϵ for Jacobian operator of a function.

means when ϵ goes to zero, the compression coefficient goes to one (uniform grid). The solution and its adaptive grid using MAWCM with Runge–Kutta time integration scheme after 10 days are plotted in Fig. 11 for $\epsilon = 10^{-5}$. The adaptive grid captures the solution very well, moreover it can clearly reflect the behavior of the function, which is the strength of MAWCM.

In order to evaluate the performance of the scheme we calculated the conservation errors for total mass and potential enstrophy defined, by the following relations

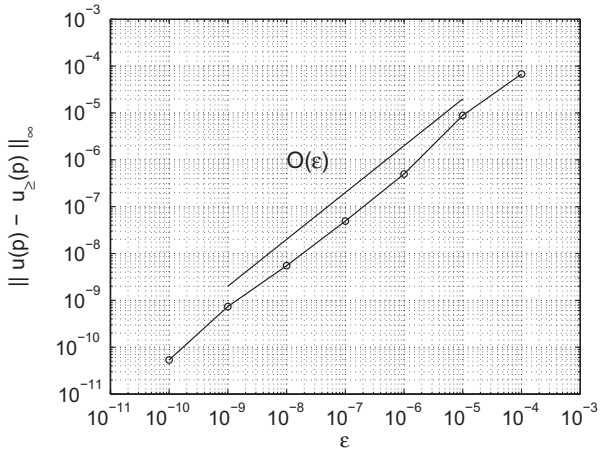

Fig. 8. Relation between ϵ end error $(\|u(p) - u_{\geqslant}(p)\|_{\infty})$ for initial vorticity equation (20).

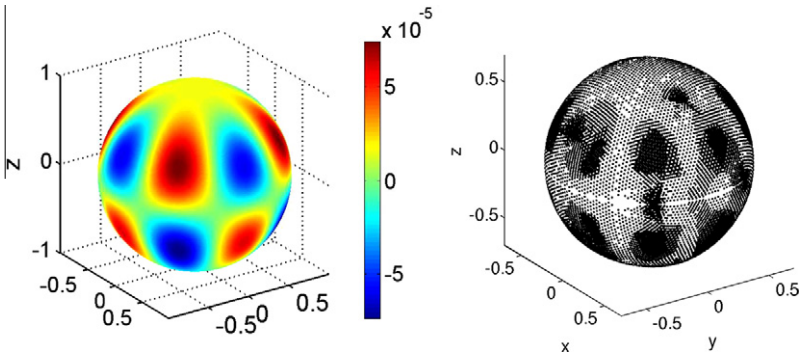

Fig. 9. Initial vorticity (ζ) (left) and its adaptive grid (right) at $t = 0$.

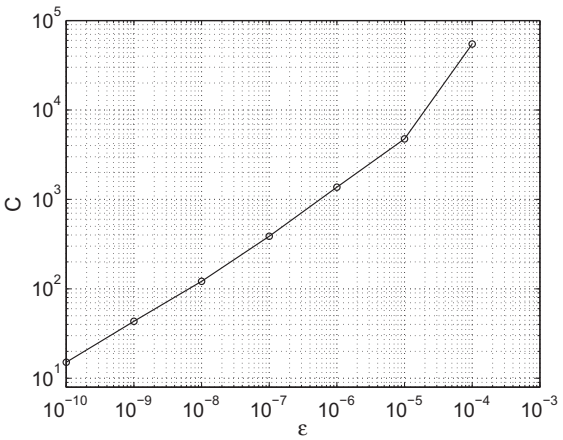

Fig. 10. Relation between compression coefficient $\mathcal{C}$ and ϵ for vorticity at time $t = 0$.

$$\text{Mass} = h, \tag{21}$$

$$\text{Potential Enstrophy} = \frac{1}{2gh}(\zeta + f)^2, \tag{22}$$

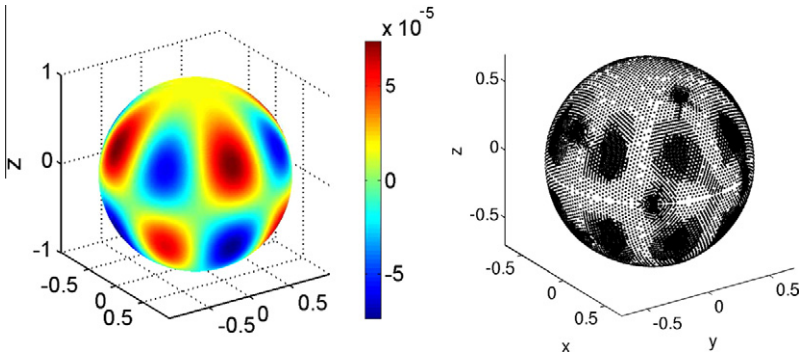

Fig. 11. Solution (left) and its adaptive grid (right) after 10 days.

where *gh* is defined by Williamson et al. [35], the conservation error is calculated using the following equation

$$\mathcal{M} = \frac{\mathcal{I}(f(\theta,\phi,t)) - \mathcal{I}(f(\theta,\phi,t=0))}{\mathcal{I}(f(\theta,\phi,t=0))}, \tag{23}$$

where $\mathcal{I}$ denotes the integral over the sphere and $f(\theta,\phi,t)$ can be total mass or potential enstrophy. In particular, the solution of non-divergent barotropic vorticity equation is in this form of traveling around the earth from west to east with constant angular velocity and the initial structure is well maintained with only minimal vacillations in shape. Moreover, the conservation errors of mass and potential enstrophy are presented in Fig. 12 (left) and (right), respectively. It is shown that the mass is fully conserved consistently and the errors for the potential enstrophy are of the same order see Fig. 12 (right).

5.3. Test case-2

In this section we consider a test case (Dipole Modon test by Verkley [14]) which solution is more localization of barotropic vorticity equation. The solution can be written as

$$\psi(\theta,\phi,t) = X(\theta',\phi') - \omega_0 \sin(\phi) + D_0, \tag{24}$$

here ω_0 is angular velocity of solid-body rotation in outer region of the modon, D_0 is the constant. Moreover (θ',ϕ') is a rotated coordinate system, which has the north pole at (θ_a,ϕ_a) with respect to the unrotated (θ',ϕ') coordinate system (see [14])

$$X(\theta',\phi') = X^d(\phi')\cos(\theta') + X^m(\phi'), \tag{25}$$

where $X^d(\phi')$ and $X^m(\phi')$ are given by

$$X^d(\phi') = (\omega_0 - C_0)\cos(\phi_a)\cos(\phi_0)F^d(\phi'), \tag{26}$$
$$X^m(\phi') = (\omega_0 - C_0)\cos(\phi_a)\sin(\phi_0)F^m(\phi'), \tag{27}$$

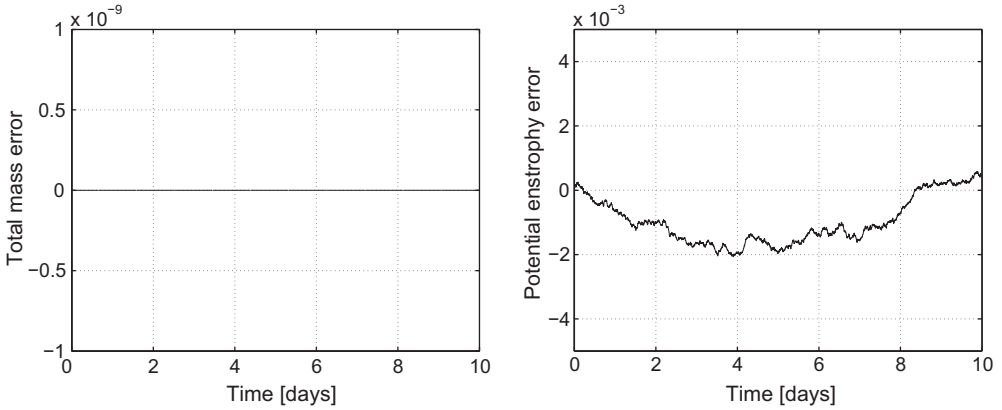

Fig. 12. Conservation of mass and enstrophy of Rossby wave test cases (left) and (right), respectively.

where ϕ_0 is the (θ,ϕ) – latitude of the modon center, and ϕ_a is the (θ',ϕ') – latitude separating the inner and outer parts of the modon, C_0 is the modon velocity. This expressions the functions $F^d(\phi')$ and $F^m(\phi')$ are given by

$$F^d(\phi') = \begin{cases} F_o^d & \text{if } \phi' \leqslant \phi_a, \\ F_i^d & \text{if } \phi' > \phi_a, \end{cases}$$

similarly we can define

$$F^m(\phi') = \begin{cases} F_o^m & \text{if } \phi' \leqslant \phi_a, \\ F_i^m & \text{if } \phi' > \phi_a, \end{cases}$$

Where

$$F_o^d(\phi') = \frac{P^1_{-1/2+ik}(-\sin(\phi'))}{P^1_{-1/2+ik}(-\sin(\phi_a))}, \tag{28}$$

$$F_o^m(\phi') = -\frac{P^0_{-1/2+ik}(-\sin(\phi'))}{P^1_{-1/2+ik}(-\sin(\phi_a))}, \tag{29}$$

$$F_o^d(\phi') = -b\frac{P^1_\alpha(\sin(\phi'))}{P^1_\alpha(\sin(\phi_a))} + (1+b)\frac{\cos(\phi')}{\cos(\phi_a)}, \tag{30}$$

$$F_o^m(\phi') = -b\frac{P^0_\alpha(\sin(\phi'))}{P^1_\alpha(\sin(\phi_a))} - (1+b)\left[\frac{\sin(\phi')-\sin(\phi_a)}{\cos(\phi_a)}\right] - \frac{P^0_{-1/2+ik}(-\sin(\phi_a))}{P^1_{-1/2+ik}(-\sin(\phi_a))} + b\frac{P^0_\alpha(\sin(\phi_a))}{P^1_\alpha(\sin(\phi_a))}, \tag{31}$$

where $b = \frac{(k^2+\frac{1}{4})+2}{\alpha(\alpha+1)-2}$ and $P_\nu^m(\sin(\phi))$is the Legendere function of non-negative order m and any arbitrary complex number ν defined by Verkley [14]. For Eq. (24) on a sphere we define $k = 10, \alpha = 10$ and $\phi_a = 1.1543(66.14^\circ)$ and $D = 0$ and $\phi_0 = 0$ at time t where $\theta_0 = \pi$.

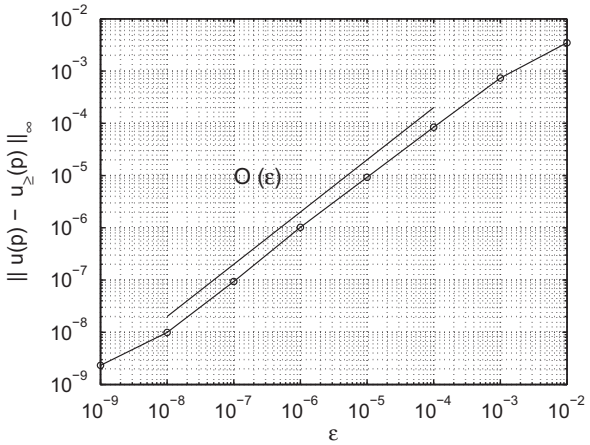

Fig. 13. Relation between ϵ and error $(\|u(p)-u_{\geqslant}(p)\|_\infty)$ at time $t = 0$ for Eq. (24).

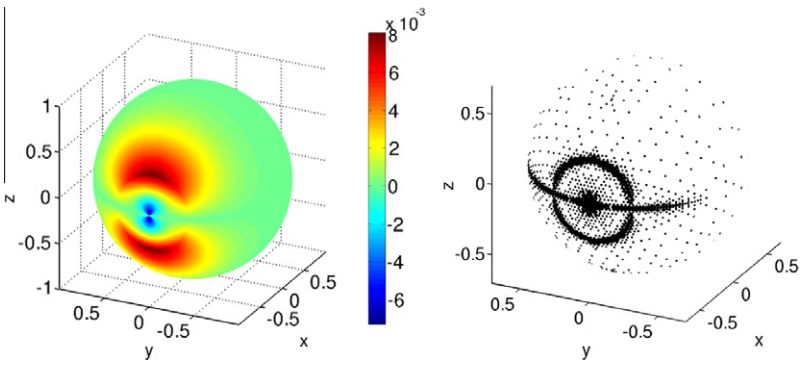

Fig. 14. Initial modon (left) and its adaptive grid (right).

Here we take Eq. (24) at time $t = 0$ and plot the relation between ϵ and error, see in Fig. 13. Furthermore, we also plotted initial solution $(t = 0)$ its adaptive grid in Fig. 14 left and right respectively. Moreover, compression coefficient $\mathcal{C} = 87$. Again in Fig. 15, is cleared that compression coefficient $\mathcal{C}$ increases when wavelet prescribed threshold parameter (ϵ) increases, means when ϵ goes to zero, the compression coefficient goes to one (uniform grid). The solution and its adaptive grid using MAWCM with Runge–Kutta time integration scheme after 10 days are plotted in Fig. 16 for $\epsilon = 10^{-4}$. Here the adaptive grid captures the solution very well which is the strength of MAWCM. In particular, the solution of non-divergent barotropic

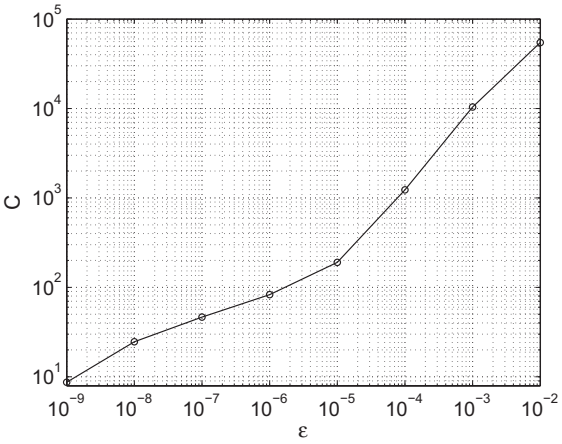

Fig. 15. Relation between compression coefficient $\mathcal{C}$ and ϵ for Eq. (24) at time $t = 0$.

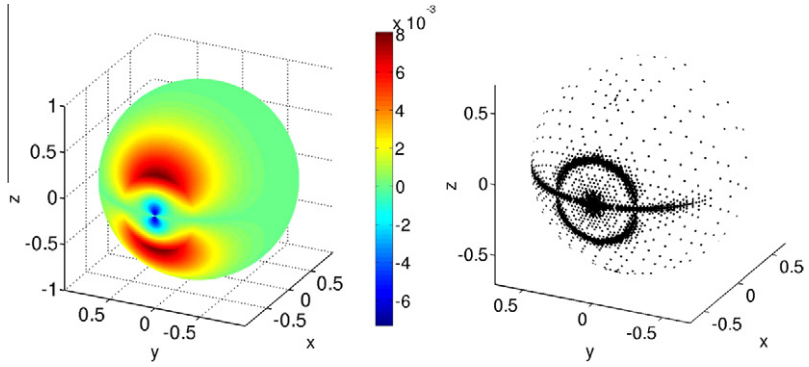

Fig. 16. After 10 days modon (left) and its adaptive grid (right).

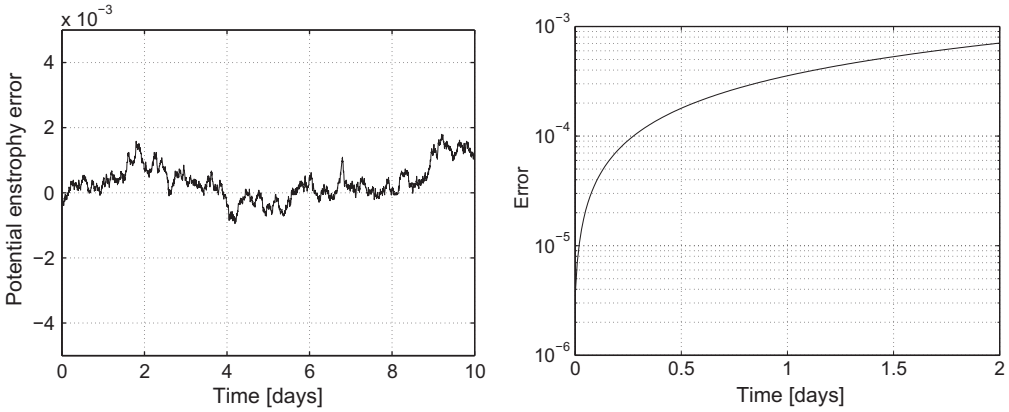

Fig. 17. Time evolution of the normalized conservation of potential enstrophy (left) and time series error (right) for test case-2.

vorticity equation is in this form of traveling around the earth from west to east with constant angular velocity and the initial structure is well maintained with only minimal vacillations in shape. Moreover, the conservation errors of potential enstrophy are presented in Fig. 17 (left). It is shown that the errors for the potential enstrophy are of the same order. Furthermore we also computed time series error see in Fig. 17 (right).

6. Summary and future work

The conclusion is that the numerical integration of the non divergent barotropic vorticity equation on an adaptive grid in our MAWCM (falls in the category of the wavelet based methods) gives very good approximate solution for chosen initial conditions. This non-divergent barotropic equation is our primary test for this method. The future importants of this MAWCM on sphere can be extension to the primitive equations for large scale motion of the atmosphere as well as small scale.

Acknowledgments

This research work was supported by Department of Science and Technology, India, under the Grant No. RP02417. The second author would also like to thanks Prof. Nicholas Kevlahan, McMaster University for introducing adaptive wavelet collocation method on the sphere. Finally the authors would like to thank the referees for their thorough reports and for pointing out oversights the original submission. Their constructive comments have led to a much improved paper.

References

[1] O.V. Vasilyev, Solving multi-dimensional evolution problems with localized structure using second generation wavelets, Int. J. Comput. Fluid Dyn. 17 (2) (2003) 151–168.
[2] R.T. Williams, J.C.L. Chan, Analytical and numerical studies of the beta-effect in tropical cyclone motion. part i: zero mean flow, J. Atmos. Sci. 44 (9) (1987) 1257–1265.
[3] M. DeMaria, Tropical cyclone motion in a nondivergent barotropic model, Mon. Weather Rev. 113 (7) (1985) 1199–1210.
[4] C.G. Rossby, On displacements and intensity changes of atmospheric vortices, J. Mar. Res. 7 (1948) 175–187.
[5] J.Y. Han, S.E. Shin, J.J. Baik, On the critical separation distance of binary vortices in a nondivergent barotropic atmosphere, J. Meteorol. Soc. Jpn. 84 (5) (2006) 853–869.
[6] C.A. Riegel, W.L. Gates, A study of numerical errors in the integration of barotropic flow on a spherical grid, J. Geophys. Res. 67 (2) (1962) 773–784.
[7] D.L. Williamson, Integration of the barotrophic vorticity equation on a spherical geodesic grid, Tellus 4 (1968) 642–653.
[8] R. Sadourny, A. Akakawa, Y. Mintz, Integration of the nondivergent baratropic vorticity equation with an icosahedral–hexagonal grid for the sphere, Mon. Weather Rev. 96 (1968) 351–356.
[9] Ramachandran D. Nair, Michael N. Levy, Henry M. Tufo, A high-order element-based Galerkin method for the barotropic vorticity equation, Int. J. Numer. Meth. Fluids (2008).
[10] D.L. Williamson, Integration of the primitive baratropic model over a spherical geodesic grid, Mon. Weather Rev. 98 (1969) 512–520.
[11] J.C. Mc Williams, N.J. Zabusky, Interactions of isolated vortices, Geophys. Astrophys. Fluid Dyn. 19 (1982) 207–227.
[12] Yuri N. Skiba, Julian Adem, On the linear stability study of zonal incompressible flows on a sphere, Numer. Methods Partial Differ. Eq. 14 (1998) 649–665.
[13] P.D. Thompson, A generalized class of exact time dependent solution of the vorticity equation for non-divergent barotrophic flow, Mon. Weather Rev. 110 (1982) 1321–1324.
[14] W.T.M. Verkley, The construction of barotropic modon on a sphere, J. Atmos. Sci. 41 (16) (1984) 2492–2504.
[15] J.J. Tribia, Modons in spherical geometry, Geophys. Astrophys. Fluid Dyn. 30 (1984) 131–168.
[16] J.A. Pudykiewicz, On numerical solution of the shallow water equations with chemical reactions on icosahedral geodesic grid, J. Comput. Phys. 230 (2011) 1956–1991.
[17] Ismael Perez Garcia, Y.N. Skiba, Simulation of exact barotropic vorticity equation solutions using spectral model, Atmosfera 12 (1999) 223–243.
[18] Kai Schneider, Oleg V. Vasilyev, Wavelet methods in computational fluid dynamics, Annu. Rev. Fluid Mech. 42 (2010) 473–503.
[19] M. Mehra, N.K.R. Kevlahan, An adaptive wavelet collocation method for the solution of partial differential equation on the sphere, J. Comput. Phys. 227 (2008) 5610–5632.
[20] S. Bertoluzza, Adaptive wavelet collocation for the solution of steady-state equations, in: SPIE Proceedings, vol. 2491, 1995, pp. 947–956.
[21] O.V. Vasilyev, C. Bowman, Second generation wavelet collocation method for the solution of partial differential equations, J. Comput. Phys. 165 (2000) 660–693.
[22] O.V. Vasilyev, N.K.-R. Kevlahan, An adaptive multilevel wavelet collocation method for elliptic problems, J. Comput. Phys. 206 (2005) 412–431.
[23] N. Kevlahan, O. Vasilyev, An adaptive wavelet collocation method for fluid–structure interaction at high Reynolds numbers, SIAM J. Sci. Comput. 26 (6) (2005) 1894–1915.
[24] M. Mehra, N.K.R. Kevlahan, An adaptive multilevel wavelet solver for elliptic equations on an optimal spherical geodesic grid, SIAM J. Sci. Comput. 30 (6) (2008) 3073–3086.
[25] I. Daubechies, Ten Lectures on Wavelets, SIAM, 1992.
[26] G. Beylkin, R. Coifman, V. Rokhlin, Fast wavelet transforms and numerical algorithms, Comm. Pure Appl. Math. 44 (1991) 141–183.
[27] Y. Meyer, Analysis at Urbana I: Analysis in Function Spaces, Cambridge University Press, Cambridge, 1989.
[28] P. Goupillaud, A. Grossman, J. Morlet, Cycle-octave and related transforms in seismic signal analysis, Geoexploration 23 (1984) 85–102.
[29] W. Sweldens, The lifting scheme: a construction of second generation wavelets, SIAM J. Math. Anal. 2 (29) (1998) 511–546.
[30] P. Schroder, W. Sweldens, Spherical wavelets: efficiently representing functions on the sphere, in: Proceedings of the 22nd Annual Conference on Computer Graphics and Interactive, Techniques, 1995, pp. 161–172.
[31] David L. Donoho, Interpolating wavelet transforms, Technical Report 408, Department of Statistics, Stanford University, 1992.
[32] G. Xu, Discrete Laplace–Beltrami operator on sphere and optimal spherical triangulation, Int. J. Comp. Geom. Appl. 16 (2006) 75–93.
[33] M. Meyer, M. Desbrun, P. Schroder, A. Barr, Discrete differential geometry operator for triangulated 2-manifolds, in: Visualization and Mathematics, vol. III, 2002, pp. 35–57.
[34] R. Heikes, D.A. Randall, Numerical integration of the shallow-water equations on a twisted icosahedral grid. Part: Basic design and results of test, Mon. Weather Rev. 123 (1995) 1862–1880.
[35] D.L. Williamson, J.B. Drake, J.J. Hack, P.N. Swarztrauber, R. Jacob, A standard test set for numerical approximations to the shallow water equations in spherical geometry, J. Comput. Phys. 102 (1992) 211–224.